ResearchGate

See discussions, stats, and author profiles for this publication at: https://www.researchgate.net/publication/258101008

Mercury–Cadmium–Telluride Waveguides – A Novel Strategy for On-Chip Mid-Infrared Sensors

ARTICLE *in* ANALYTICAL CHEMISTRY · OCTOBER 2013

Impact Factor: 5.64 · DOI: 10.1021/ac4025544 · Source: PubMed

CITATIONS
8

READS
65

6 AUTHORS, INCLUDING:

Xiaofeng Wang
Universität Ulm
4 PUBLICATIONS **49** CITATIONS
SEE PROFILE

Boris Mizaikoff
Universität Ulm
311 PUBLICATIONS **4,800** CITATIONS
SEE PROFILE

Available from: Boris Mizaikoff
Retrieved on: 31 January 2016

analytical chemistry

Letter

pubs.acs.org/ac

Mercury–Cadmium–Telluride Waveguides – A Novel Strategy for On-Chip Mid-Infrared Sensors

Xiaofeng Wang,[†] Jarek Antoszewski,[‡] Gino Putrino,[‡] Wen Lei,[‡] Lorenzo Faraone,[‡] and Boris Mizaikoff*[,†]

[†]Institute of Analytical and Bioanalytical Chemistry, University of Ulm, Albert-Einstein-Allee 11, 89075 Ulm, Germany

[‡]Microelectronics Research Group, Department of Electrical and Electronic Engineering, University of Western Australia, Perth, WA 3182, Australia

Supporting Information

ABSTRACT: We report the first planar waveguides made from mercury–cadmium–telluride (MCT)—a material to date exclusively used for mid-infrared (MIR) detector elements—serving as on-chip MIR evanescent field transducers in combination with tunable quantum cascade lasers (tQCLs) emitting in the spectral regime of 5.78–6.35 μm. This novel MIR sensing approach utilizes structured MCT chips fabricated via molecular beam epitaxy (MBE) as waveguide enabling sensing via evanescent field absorption spectroscopy, as demonstrated by the detection of 1 nL of acetone. Complementary finite difference time domain (FDTD) simulations fit well with the experimentally obtained data and predict an improvement of the limit of detection by at least 2 orders of magnitude upon implementation of thinner MCT waveguides. With the first demonstration of chemical sensing using on-chip MCT waveguides, monolithically fabricated IR sensing systems directly interfacing the waveguide with the MCT detector element may be envisaged.

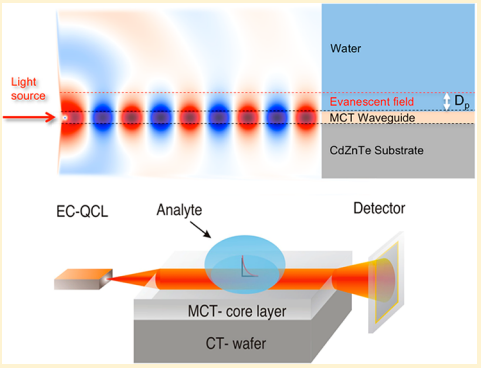

Mid-infrared (MIR; 3–20 μm) spectroscopy is based on the excitation of vibrational and rotational modes associated with most organic and inorganic molecules absorbing MIR photons, and provides inherent molecular selectivity. Hence, this spectral regime is particularly attractive for optical sensing applications.[1] Despite its inherent potential, most applications of MIR spectroscopy, and in particular analytical scenarios probing liquid phase environments, remain confined to appropriately equipped laboratories due to the dimensions of conventional IR spectroscopic equipment.[2] Considering the already achieved level of miniaturization/integration of UV–vis and near-infrared (NIR) optical devices, the opportunities for miniaturization in MIR sensor and photonics technology are evident enabling in situ and on-site chem/bio monitoring, sensing, and surveillance. However, viable strategies enabling miniaturizing/integrating each optical component of the sensing system are required in order to facilitate on-chip MIR sensor technology for advanced portable sensing systems.[3]

Waveguide-based MIR sensing systems generally comprise four major components: (i) an MIR radiation source, (ii) waveguides for propagating the radiation and frequently also serving as the transducer, (iii) a wavelength selection device, and (iv) an MIR detector. Among the available MIR radiation sources, quantum cascade lasers are nowadays widely accepted as the most advanced light source in IR sensing.[4,5] In brief, QCLs are semiconductor lasers generating light emission via intersubband transitions of electrons in the conduction band within a series of quantum heterostructures, rather than conventional electron–hole recombination.[6] QCLs provide high output power within narrow spectral bands, compact dimensions (i.e., few hundreds of micrometers), a long lifetime, tunable emission (in part exceeding 200 cm^{-1}), and access to almost the entire MIR spectral range.[7,8] The utility of QCLs in waveguide-based evanescent field absorption sensing has recently been demonstrated in a variety of liquid phase application scenarios.[9−11]

In the MIR regime, condensed phase sensing frequently takes advantage of total internal reflection (i.e., evanescent field absorption) spectroscopy based on conventional attenuated total reflection (ATR) crystals or infrared transmitting optical fibers.[12] The evanescent field generated at the waveguide-sample interface interacts with IR absorbing analytes present within the penetration depth of the evanescent field, and results in attenuation of the propagating wave at analyte-specific absorption frequencies. The evanescent field penetrates with exponentially decaying intensity a few micrometers into the adjacent medium and is, thus, particularly capable of probing analytes present in IR-opaque media such as water within this quasi thin-film cell. The absorption within the evanescent field follows a pseudo Lambert–Beer relationship $A = (\varepsilon cl)\, r$, where ε is the molar absorptivity, c is the concentration of the analyte, l is the equivalent optical path length, and r is the fraction of power residing outside the waveguide core. Consequently,

Received: August 11, 2013
Accepted: October 25, 2013
Published: October 25, 2013

 © 2013 American Chemical Society

enhancing the intensity of the evanescent field directly affects the obtainable signal-to-noise ration (SNR) of the absorption measurement, and, thus, the achievable sensitivity. The intensity of the evanescent field is dependent on the dielectric constant at the interface waveguide sample, and on the cross-sectional dimensions of the waveguide, which affects the mode propagation. As the dielectric constant is determined by the involved materials, the most significant sensitivity gain is expected from smartly tailoring and optimizing the waveguide structure and geometry.

Infrared transmitting fibers are usually fabricated from a limited set of IR-transparent materials dominated by polycrystalline silver halides (AgBr−AgCl, usually abbreviated as AgX),[13] and amorphous chalcogenide glasses (As−Se−Te).[14] For example, the research group of Gmachl has reported progress in liquid-phase sensing by combining QCLs with silver halide fiber segments.[9] Recently, single-mode fibers transparent up to a wavelength of 4.5 μm have been reported along with single-mode planar waveguides.[15,16] The group of Mizaikoff and collaborators has reported a new generation of semiconductor (GaAs/AlGaAs) thin-film IR waveguides grown by molecular beam epitaxy (MBE) extending the useful spectral window up to 13 μm, yet maintaining single-mode behavior.[11] Recently, a new generation of strip waveguides has been microfabricated from GaAs/AlGaAs semiconductor wafers, thereby demonstrating excellent analytical performance probing minute sample amounts with unsurpassed sensitivity via evanescent field sensing.[17] Very recently, the first mid-infrared Mach−Zehnder interferometers (MIR-MZI) combined with a broadly tunable quantum cascade laser (tQCL) as an example of more delicate optical structures have been developed.[18]

In the present study, epitaxially grown thin-film planar MCT waveguides are reported serving as a transducer for MIR chemical sensing applications. Both simulations and experiments reveal the outstanding optical/analytical performance of MCT waveguides promising highly miniaturized MIR optical sensor platforms in combination with tQCLs. Based on these findings, chip-level monolithic integration of MIR waveguides/transducers with MCT detectors may be envisaged for the first time.

FDTD SIMULATIONS

Two-dimensional finite difference time domain (FDTD) simulations of the proposed waveguide structure were performed using MEEP.[19] The basic structure that was simulated comprises a planar photonic waveguide immersed in an aqueous solution (i.e., refractive index 1.3). The waveguide itself is modeled at a substrate surface. Infrared light was coupled into the waveguide and propagated through the structure. In the FDTD model, a TE polarized point source radiating at a wavelength of 6 μm was used as a simple light source model launching radiation into the waveguide. A perfectly matched layer (PML) at the boundary of the simulated geometry was simulated to absorb light emitted by the virtual light source that is not coupled into the waveguide layer. Consequently, only light guided within the waveguide along the propagating direction contributes to the final considerations on the field distribution. Figure 1a shows the resulting optical field in an exemplary structure of HgCdTe/CdZnTe modeled for a light source emitting radiation at 6 μm.

Along the direction of photon propagation within the MCT waveguide, the color scale changes from blue (i.e., negative electric field) to white (i.e., zero field), and then to red (i.e., positive electric field). As expected, the main fraction of the radiation is confined inside the waveguide. At the interface between the waveguide and water, the evanescent electrical field is evident. The evanescent field decreases exponentially in intensity with increasing distance from the interface into the ambient media. The penetration depth of the evanescent field (d_p) is defined as the distance from the interface at which the power of the electric field has decreased to $1/e$ of its initial value. From the model, a penetration depth of the evanescent field of 0.8 μm (@ λ = 6 μm) can be calculated given the present configuration.

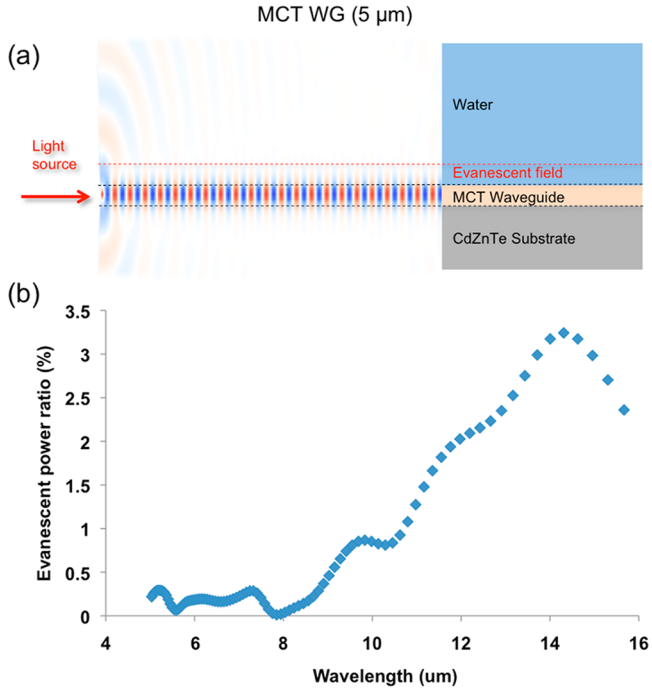

Figure 1. FDTD modeling of MIR propagation through a 5 μm thick MCT waveguide: (a) Optical field distribution along a HgCdTe/CdZnTe slab waveguide. The MCT layer has a refractive index of n = 3.5, and the CdZnTe substrate has a refractive index of 2.7. (b) Evanescent power ratio in the 5−16 μm spectral region shown as the percentage of the optical power within the evanescent field (i.e., interacting with the adjacent sample medium) vs the total optical power coupled into the waveguide.

Further calculations of the evanescent power ratio across a broad MIR spectral window (5−16 μm) are shown in Figure 1 b. It is evident that the optical power within the evanescent field does not steadily increase with increasing wavelength, in particular at the shorter wavelength regime. This may be explained by the fact that multimode photon propagation is supported at the relatively large core waveguide layer dimensions, especially with decreasing wavelength vs core waveguide diameter. For designing optimized mode-matched MCT waveguide structures with enhanced evanescent field intensities, a series of MCT waveguides were modeled and compared to already existing GaAs/AlGaAs waveguides, as shown in the Supporting Information.

EXPERIMENTAL RESULTS

The MCT waveguides were grown via MBE on $Cd_{0.96}Zn_{0.04}Te$ substrates at a growth temperature of 185 °C using appropriate sources. The epitaxial growth of the MCT layer was terminated at a thickness of 5 μm. The MCT layer was analyzed with a

dx.doi.org/10.1021/ac4025544 | Anal. Chem. 2013, 85, 10648−10652

calibrated MIR light source, and a refractive index of n = 4.0 at 5.2 μm was determined. A selectively grown CdTe layer on top of the MCT layer serves as a protective layer. The CdTe layer has a refractive index of n = 2.7 at 5.2 μm.

The MCT wafer (1 × 1 cm^2) was cleaved along the crystal axis, thus providing a waveguide chip with a footprint of 1 × 0.8 cm^2. In Figure 2, a scanning electron microscopy (SEM) image

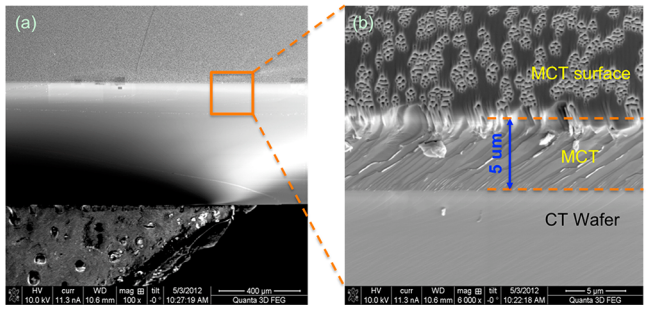

Figure 2. SEM study at HgCdTe/CdZnTe waveguide grown on a CdTe wafer substrate. (a) Cross section of the waveguide along crystal axis of the CT wafer; (b) magnified view of the layer interface revealing the contrast between the 5 μm thick MCT core layer and the CdTe wafer substrate. Structures evident at the surface of the waveguide within the magnified view are resulting from the cleaving process.

of an exemplary waveguide cross section is shown visualizing the individual layers via their material contrast. The cleaved end-facet also shows sufficient surface quality ensuring efficient optical coupling at minimum scattering losses.

The IR sensor setup was composed of a tunable QCL light source (Daylight Solutions Inc., San Diego, CA, USA) providing MIR radiation in the spectral range 5.78−6.35 μm (1570−1735 cm^{-1}) at a spectra resolution of 0.01 cm^{-1}. The collimated laser radiation was focused via a ZnSe lens onto the end facet of the MCT planar waveguide. MIR photons were propagated along the core waveguide layer and coupled out at the distal end of the waveguide. Radiation emitted at that waveguide facet was refocused by a pair of ZnSe lenses onto a mercury−cadmium−telluride (MCT) detector (Kolmar Technologies, Newbury, MA, USA) cooled with liquid nitrogen, which was connected to an oscilloscope. The amplitude of the transmitted laser light intensity was recorded for further data processing. During experiments, an aperture was applied at both ends of the MCT waveguide structure revealing only the waveguide core facet, thereby eliminating contributions via scattered (nonguided) radiation. Figure 3a shows the MCT on-chip waveguide with the incoupling/outcoupling ZnSe lenses aligned using 3-D translational stages, while Figure 3b schematically illustrates the IR beam path.

The waveguide structure designed herein supports single-mode propagation. At the MCT core waveguide interface with the optically rare adjacent medium (e.g., air or liquid sample), an exponentially decaying evanescent field is generated, as schematically indicated in Figure 3b. Hence, MIR radiation may interact with absorbing analytes present within a sample solution deposited on top of the waveguide surface, thereby attenuating the transmitted radiation via evanescent field absorption as a function of the surface coverage and of the concentration of the absorbing species.

Planar GaAs/AlGaAs slab waveguides, currently the only alternative MIR semiconductor waveguide technology, cleaved

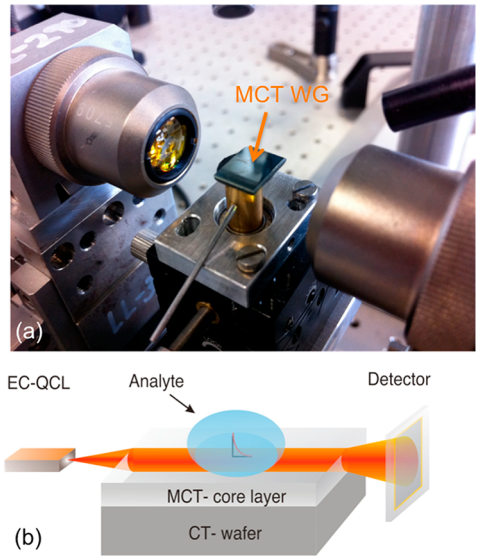

Figure 3. Experimental IR sensor setup combining an MCT waveguide with a tQCL. (a) MCT translational stage with a pair of ZnSe lenses (0.5″ focal length). (b) Schematic light propagation via MCT core waveguiding layer and interaction of analyte droplet with the evanescent field. During experiments, an aperture was applied at both ends of the MCT waveguide structure revealing only the waveguide core facet, thereby eliminating contributions via scattered (nonguided) radiation.

from an epitaxially grown wafer at similar dimensions were used for sensitivity comparisons. The $Al_{0.2}Ga_{0.8}As$ cladding layer has a refractive index of 3.2 (vs 3.3 for the core waveguide) at 5.8 μm and serves as an optical buffer between the 6 μm core GaAs layer serving as the actual waveguide and the n-doped GaAs substrate.[17]

For establishing a calibration based on MCT waveguide-based IR sensor prototypes, diluted solutions of acetone in isopropanol were prepared. Isopropanol was selected as the solvent due to its transparency in the required MIR spectral window at 1710 cm^{-1}, where a characteristic absorption peak of acetone is located. The tQCL was therefore adjusted to emit at 1710 cm^{-1} (i.e., 5.8 μm) in pulsed mode (applied current: 833 mA; emitted peak power: 230 mW). A volume of 0.2 μL of analyte solution was added via an Eppendorf pipet in the center of the MCT waveguide surface. After deposition, the surface tension caused the droplet to spread at the waveguide surface resulting in a circular surface coverage with a diameter of approximately 3 mm, which ensures that the entire evanescent field across the beam waist is addressed. The propagation path of the IR beam within the MCT waveguide was analyzed as shown during previous studies.[17]

The series of analyte droplets deposited at the surface had concentrations of 1.36, 2.72, 4.08, 5.44, 6.81, and 13.62 M of acetone in isopropanol comprising a volume of 0.02, 0.04, 0.06, 0.08, 0.1, and 0.2 μL, respectively. Correspondingly, the intensity of the radiation propagating through the waveguide was dampened via evanescent field absorption following $A = \log(I/I_0)$. The relationship between absorbance and concentration is shown in Figure 4. A linear fit (r^2 of 0.996) is obtained; the error bars (each measurement was repeated 3 times and averaged) associated with these measurements are mainly attributed to the manual deposition of the droplets. The actual contribution of the absorption results exclusively from the very thin liquid film at the sample−waveguide interface,

dx.doi.org/10.1021/ac4025544 | Anal. Chem. 2013, 85, 10648−10652

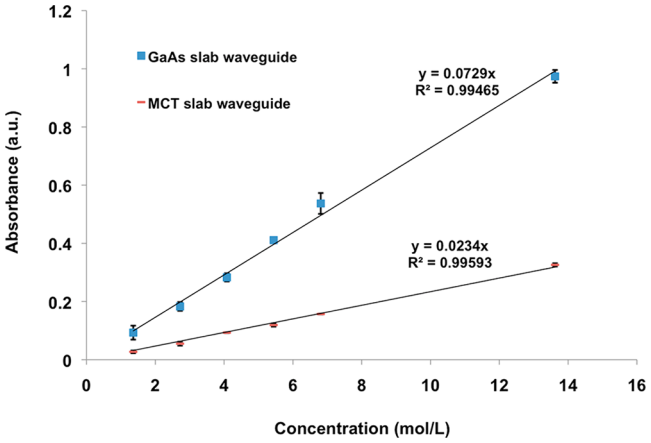

Figure 4. Sensor response to solutions of acetone dissolved in isopropanol deposited at the MCT slab waveguide and at a GaAs slab waveguide surface. Each 0.2 μL droplet resulted in a circular surface deposit with a diameter of approximately 3 mm.

and, more precisely, from the volume of analyte resulting in a coverage length of 3 mm along the waveguide surface considering a waist of the propagating beam below 1 μm and a penetration depth of the evanescent field of 0.8 μm. This results in a reliable detection of approximately 1 nL (i.e., 791 ng) of actone. On the basis of the 3σ-criterion, the lowest detectable volume was calculated at 90 pL (i.e., 71.1 ng).

Similar studies were performed using a planar GaAs/AlGaAs slab waveguide. Here, 0.2 μL of analyte solution prepared the same way as described above was deposited at the center of the GaAs waveguide surface. The obtained calibration functions for the MCT and the GaAs waveguides are compared in Figure 4. While the slope of the obtained linear calibration function is apparently steeper for the GaAs-based IR sensor, the obtained limits of detection are basically en par; i.e., the performance of the first prototype MCT waveguide is almost at the same level as the GaAs waveguide. Considering the modeling results (see also Supporting Information), these first MCT thin-film chips are not yet optimized for evanescent field sensing, as the sensitivity could be significantly improved by further decreasing the core MCT waveguide thickness below 1 μm.

CONCLUSIONS

In the present study, first mercury−cadmium−telluride semiconductor waveguides have been designed and fabricated serving as a thin-film waveguide for MIR evanescent field liquid phase sensing combined with tunable QCLs. Most importantly, these types of semiconductor waveguides share their material composition with MCT detectors, which are the most commonly applied photoconductive IR detection devices. Exemplarily, the detection of acetone dissolved in isopropanol via evanescent field absorption revealed a measured LOD of 1 nL, which is competitive to the optimized GaAs/AlGaAs semiconductor waveguide. Using the 3σ-criterion, the lowest detectable volume was calculated at 90 pL.

Complementary simulations of single-mode MCT waveguides indicate that further decreasing the thickness of the waveguide core layer <1 μm should provide even more tightly confined single-mode photon propagation, thereby significantly enhancing the fraction of energy propagating within the evanescent field. Due to the optical property of the MCT waveguide material, high transmittance across the entire MIR region, and a large refractive index contrast of the core/cladding layers, an additional signal enhancement by up to 2 orders of magnitude may be predicted.

Moreover, further microstructuring of MCT waveguide chips is facilitated via conventional wet/dry etching methods commonly used in semiconductor microfabrication, which are already in use for MCT detector chip fabrication. Hence, the generation of strip or ring waveguides, as well as grating couplers or resonant structures, appears straightforward in a next development step, as already shown for UV/vis, NIR, and MIR waveguide-based devices.[20−22]

Last but not least, a monolithic sensing platform facilitating integrated waveguide and detector structures based on the MCT materials system may be envisaged promising innovative approaches toward chip-level integration for infrared chem/bio sensing devices.

ASSOCIATED CONTENT

Supporting Information

Experimental details and figures. This material is available free of charge via the Internet at http://pubs.acs.org.

AUTHOR INFORMATION

Corresponding Author

*E-mail: boris.mizaikoff@uni-ulm.de.

Notes

The authors declare no competing financial interest.

ACKNOWLEDGMENTS

The authors acknowledge the *Focused Ion Beam Center UUlm* supported by the FEI Company (Eindhoven, Netherlands), the German Science Foundation (INST40/385-F1UG), and the Struktur- und Innovationsfonds Baden-Württemberg for device prototyping and characterization. Furthermore, the authors gratefully acknowledge partial support of this study by the Kompetenznetz Funktionelle Nanostrukturen Baden Wuerttemberg, Germany.

REFERENCES

(1) Mizaikoff, B. *Anal. Chem.* **2003**, *75*, 258A−267A.
(2) Rotermund, F.; Petrov, V.; Noack, F. *Opt. Commun.* **2000**, *185*, 177−183.
(3) Kim, S.-S.; Young, C.; Mizaikoff, B. *Anal. Bioanal. Chem.* **2008**, *390*, 231−237.
(4) Kazarinov, R. F.; Suris, R. A. *Fizika i Tekhnika Poluprovodnikov (Sankt Peterburg)* **1971**, *5*, 797−800.
(5) Faist, J.; Capasso, F.; Sivco, D. L.; Sirtori, C.; Hutchinson, A. L.; Cho, A. Y. *Science* **1994**, *264*, 553−556.
(6) Saleh, B. E. A.; Teich, M. C. *Fundamentals of Photonics*, 2nd ed.; John Wiley & Sons: Hoboken, NJ, 2007; Chapter 17.
(7) Capasso, F.; Gmachl, C.; Sivco, D. L.; Cho, A. Y. *Phys. Today* **2002**, *55*, 34−40.
(8) Young, C.; Kim, S.-S.; Luzinova, Y.; Weida, M.; Arnone, D.; Takeuchi, E.; Day, T.; Mizaikoff, B. *Sens. Actuators, B* **2009**, *140*, 24−28.
(9) Chen, J.; Liu, Z.; Gmachl, C.; Sivco, D. *Opt. Express* **2005**, *13*, 5953−5960.
(10) Charlton, C.; Katzir, A.; Mizaikoff, B. *Anal. Chem.* **2005**, *77*, 4398−4403.
(11) Charlton, C.; Giovannini, M.; Faist, J.; Mizaikoff, B. *Anal. Chem.* **2006**, *78*, 4224−4227.
(12) Janotta, M.; Vogt, F.; Voraberger, H.-S.; Waldhauser, W.; Lackner, J. M.; Stotter, C.; Beutl, M.; Mizaikoff, B. *Anal. Chem.* **2004**, *76*, 384−391.

(13) Karlowatz, M.; Kraft, M.; Mizaikoff, B. *Anal. Chem.* **2004**, *76*, 2643−2648.
(14) MacDonald, S.; Michel, K.; LeCoq, D.; Boussard-Pledel, C.; Bureau, B. *Opt. Mater.* **2004**, *25*, 171−178.
(15) Grille, R.; Martin, G.; Labadie, L.; Arezki, B.; Kern, P.; Lewi, T.; Tsun, A.; Katzir, A. *Opt. Express* **2010**, *17*, 12516−12522.
(16) Houizot, P.; Boussard-Plédel, C.; Faber, A. J.; Cheng, L. K.; Bureau, B.; Van Nijnatten, P. A.; Gielesen, W. L. M.; Pereira do Carmo, J.; Lucas, J. *Opt. Express* **2007**, *15*, 12529−12538.
(17) Wang, X.; Kim, S.-S.; Rossbach, R.; Jetter, M.; Michler, P.; Mizaikoff, B. *Analyst* **2012**, *137*, 2322−2327.
(18) Sieger, M.; Balluff, F.; Wang, X.; Kim, S.-S.; Leidner, L.; Gauglitz, G.; Mizaikoff, B. *Anal. Chem.* **2013**, *85*, 3050−3052.
(19) Oskooi, A. F.; Roundy, D.; Ibanescu, M.; Bermel, P.; Joannopoulos, J. D.; Johnson, S. G. *Comput. Phys. Commun.* **2010**, *181*, 687−702.
(20) Armani, A. M.; Kulkarni, R. P.; Fraser, S. E.; Flagan, R. C.; Vahala, K. J. *Science* **2007**, *317*, 783−787.
(21) Nitkowski, A.; Chen, L.; Lipson, M. *Opt. Express* **2008**, *16*, 11930−11936.
(22) Esteban, Ó.; González-Cano, A.; Díaz-Herrera, N.; Navarrete, M.; Kim, S.-S.; Mizaikoff, B. *Plasmonics* **2012**, *7*, 647−652.

Mercury-Cadmium-Telluride Waveguides – A Novel Strategy for On-Chip Mid-Infrared Sensors

Supporting Information (SI)

Xiaofeng Wang,[†] *Jarek Antoszewski,*[‡] *Gino Putrino,*[‡] *Wen Lei,*[‡] *Lorenzo Faraone,*[‡]

Boris Mizaikoff[†]*

[†] Institute of Analytical and Bioanalytical Chemistry, University of Ulm, Albert-Einstein-Allee 11, 89075 Ulm, Germany.

[‡] Microelectronics Research Group, Department of Electrical and Electronic Engineering, University of Western Australia, Perth, WA 3182, Australia.

*Corresponding author: boris.mizaikoff@uni-ulm.de

ABSTRACT. The SI contains further FDTD modeling of a series of MCT waveguides for designing optimized single-mode MCT waveguides providing enhanced evanescent field intensities and an extended penetration depth (d_p). Furthermore, an already experimentally proven GaAs semiconductor waveguide structure was modeled for comparison.

The effect of decreasing the thickness of the HgCdTe core waveguiding layer on the intensity of the evanescent field was studied. Figure S-1 shows the electric field distribution for two exemplary MCT waveguides. By comparing the electric field distribution within the waveguide and the evanescent field for (a) a 1 µm MCT waveguide layer, and (b) a 0.5 µm MCT waveguide, it is immediately visually evident at the interface waveguide/water that a much larger fraction of the photon energy is guided outside the waveguide (i.e., within the evanescent field) with decreasing waveguide thickness. Therefore, a significant improvement of the signal-to-noise ratio during absorption measurements via the evanescent field at the waveguide surface is expected. Additionally the evanescent wave shows extended penetration into the ambient solution, as confirmed by the calculated value of d_p for each MCT waveguide in Figure S-1.

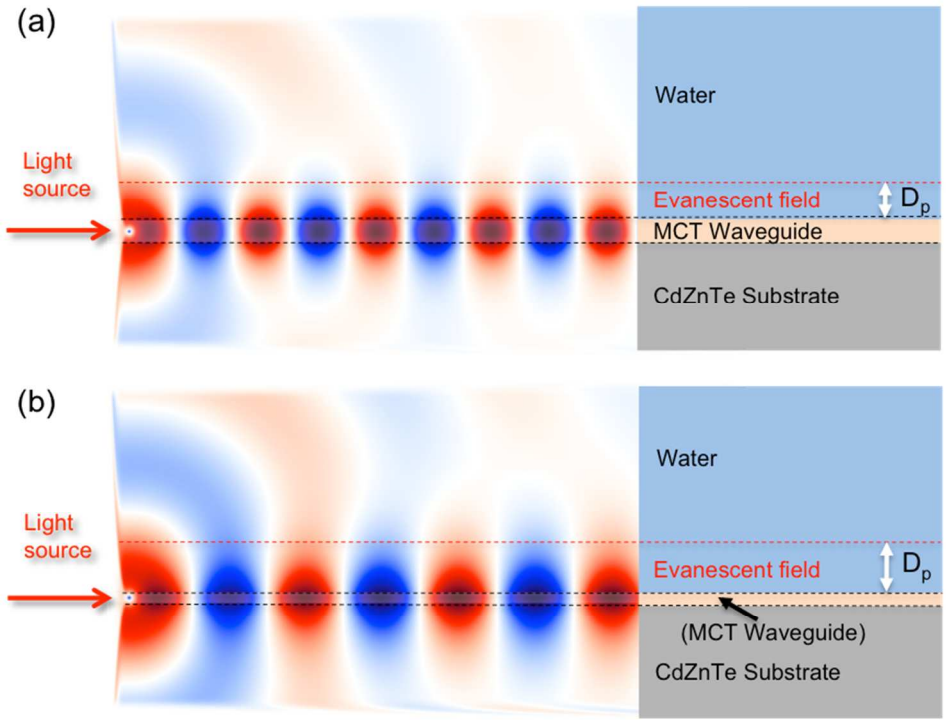

Figure S-1. Optical field distribution along HgCdTe/ CdZnTe slab waveguide with decreasing MCT waveguide layer thickness. (a) Thickness of 1 µm results in d_p = 1.4 µm; (b) thickness of 0.5 µm results in d_p = 1.8 µm.

The absorbance is proportional to *r*, the fraction of power residing outside the waveguide core. However, for the MCT waveguides studied herein it has to be considered that only the evanescent power penetrating into the sample solution (i.e., water) will contribute to the interaction with the analyte applied at the waveguide surface, while the evanescent field penetrating into the substrate will not contribute to the analytical signal. Calculations of the evanescent power ratio for the waveguides modeled in this study are shown in Figure S-2 covering a wavelength regime of 5-16 µm.

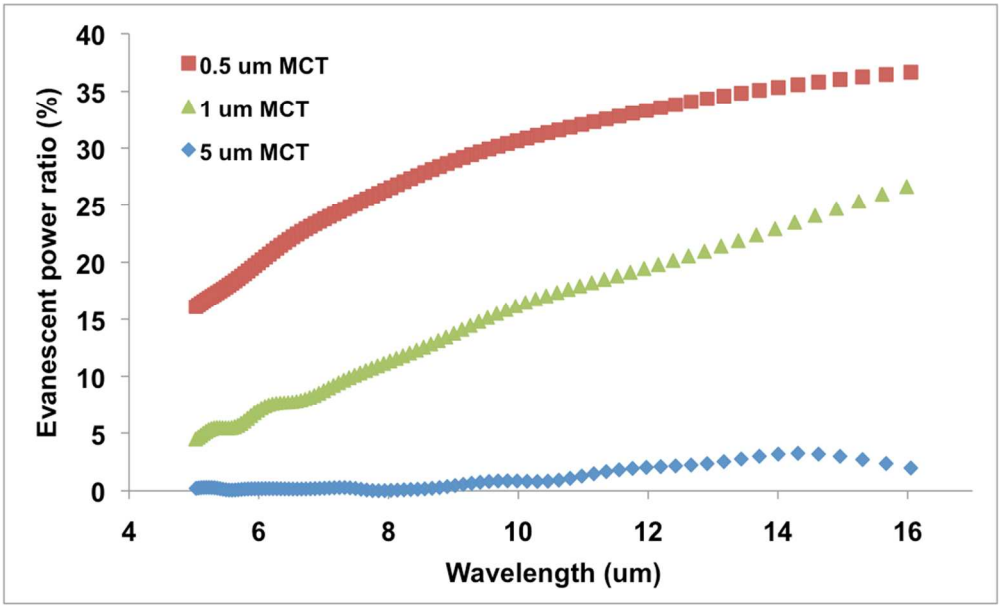

Figure S-2. Optical power ratio of the evanescent field (i.e. within the adjacent sample medium) in the 5-16 µm spectral regime shown as a percentage of the total optical power coupled into the core of the waveguide after the photons have propagated a distance of 50 µm along the waveguide.

Considering an individual wavelength, it is evident that particularly with increasing wavelength and decreasing thickness of the MCT core waveguiding layer, the optical power within the evanescent field dramatically increases. Considering $A = (\varepsilon c l)\, r$ at a wavelength of 5.8 µm, which is characteristic for the absorption of acetone analyzed as an exemplary analyte within this study, *r* (i.e. the fraction of optical power within the evanescent field) is calculated as 0.14%

(@ 5 μm MCT waveguide thickness), 6.2% (@ 1 μm MCT waveguide thickness), and 19% (@ 0.5 μm MCT waveguide thickness). Consequently, by simply decreasing the MCT core waveguiding layer thickness from 5 μm to 0.5 μm, an enhancement of the optical power by up to 2 orders of magnitude is anticipated.

Furthermore, it is evident that for each individual waveguide structure, the optical power within the evanescent field increases with increasing wavelength. Hence, the achievable enhancement is also wavelength dependent, and waveguide structure optimized for evanescent field sensing must also consider the respective emission wavelength provided by the light source. Additionally, by decreasing the thickness of the MCT layer from 1 μm to 0.5 μm, at a wavelength of 5 μm the optical power within the evanescent field is approx. 3.6-times enhanced (from 4.5 % to 16 %), whereas only a 1.4-time enhancement (from 27% to 37%) at wavelength of 16 μm may be obtained. Consequently, the achievable optical enhancement is higher at shorter wavelengths with decreasing waveguide thickness.

Finally, a GaAs/AlGaAs slab waveguide was modeled for comparison as the currently only alternative semiconductor MIR waveguide technology. This waveguide has been reported as the first single-mode IR semiconductor waveguide, and a series of analytical studies have confirmed the utility of this wafer structure [11,17,18]. The obtained photon propagation properties are shown in Figure S-3. Figure S-4 illustrates a comparison with the results obtained for the 5 μm MCT waveguide.

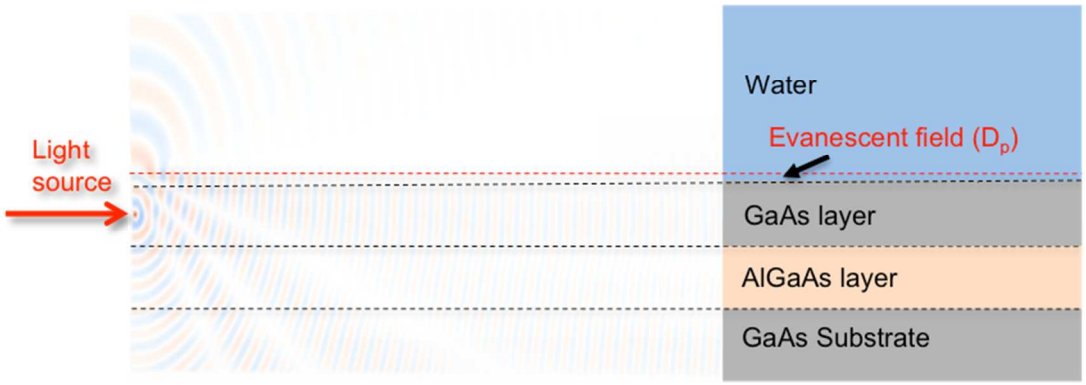

Figure 4. Optical field distribution along GaAs/ AlGaAs/GaAs slab waveguide. 6 µm GaAs core layer with refractive index n = 3.3, 6 µm AlGaAs cladding layer with n = 3.2 and doped GaAs substrate with n = 2.8 [11]. d_p is calculated to be 0.5 µm.

The optical power within the evanescent field reveals overall comparable values between the two types of waveguide material within the 5-16 µm spectral window. Moreover, it is evident that the optical power within the evanescent field does not steadily increase with increased wavelength, in particular at the shorter wavelength regime. This may be explained by the fact that multi-mode photon propagation is supported in both waveguides at this relatively large core waveguide layer dimensions. These fluctuations of the optical power within the evanescent field are evident until the wavelength is long enough such that exclusive single-mode propagation within the waveguide is ensured, or the core layer thickness supports only single-mode propagation in this frequency window, as is the case for a 0.5 µm thin MCT waveguide (see Figure S-2).

Given these considerations, the design of single-mode waveguides tailored to the emission wavelength window of any light source is readily facilitated via controlling the waveguide core layer thickness. More importantly, this strategy enables precise control on the evanescent field and the fraction of optical power within this leaky mode, which is crucial for analytical applications such as e.g. chem/bio sensors or waveguide-based bioassay technologies in the MIR.

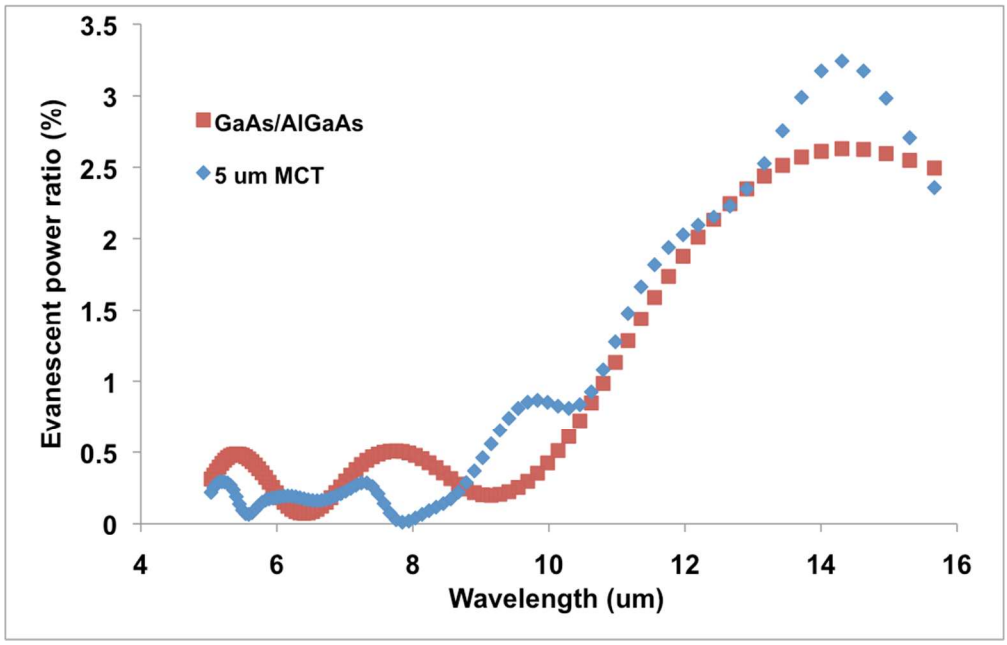

Figure S-4. Comparison of evanescent field power ratio between 6 μm GaAs/AlGaAs and 5 μm MCT slab waveguide.